Involvement of RNase J in CRISPR RNA maturation in the cyanobacterium *Synechocystis* sp. PCC 6803

Raphael Bilger[1], Friedel Drepper[2], Bettina Knapp[2], Tanja Berndt[1], Helena Landerer[1], Harald Putzer[3], Pitter Huesgen[2,4] and Wolfgang R. Hess[1,*]

[1]University of Freiburg, Faculty of Biology, Genetics and Experimental Bioinformatics, Schänzlestr. 1, D-79104 Freiburg, Germany

[2]University of Freiburg, Faculty of Biology, Biochemistry and Functional Proteomics, Schänzlestr. 1, D-79104 Freiburg, Germany …

[3]Expression Génétique Microbienne (EGM), CNRS, Université Paris Cité, Institut de Biologie Physico-Chimique, F- 75005 Paris, France

[4]University of Freiburg, CIBSS Centre for Integrative Biological Signalling Studies, D-79104 Freiburg, Germany

*Corresponding authors: Wolfgang R. Hess; Phone: +49-761-2032796; E-mail: wolfgang.hess@biologie.uni-freiburg.de

Keywords: CRISPR-Cas systems, cyanobacteria, degradosome, gene expression regulation, ribonuclease J, RNA structure, RNA:RNA interaction

Abstract

Many bacteria and archaea use CRISPR-Cas systems, which provide RNA-based, adaptive, and inheritable immune defenses against invading viruses and other foreign genetic elements. The proper processing of CRISPR guide RNAs (crRNAs) is a crucial step in the maturation of the defense complexes and is frequently performed by specialized ribonucleases encoded by *cas* genes. However, some systems employ enzymes associated with degradosome or housekeeping functions, such as RNase III or the endoribonuclease RNase E. Here, the endo- and 5´-exoribonuclease RNase J was identified as an additional enzyme involved in crRNA maturation, acting jointly with RNase E in the crRNA maturation of a type III-Bv CRISPR-Cas system, and possibly together with a further RNase in the cyanobacterium *Synechocystis* sp. PCC 6803. Co-IP experiments revealed a small set of proteins that were co-enriched with RNase J, among them the exoribonuclease polyribonucleotide nucleotidyltransferase (PNPase). Despite a measured, strong 3’ exonucleolytic activity of the recombinant enzyme, PNPase was not confirmed to contribute to crRNA maturation. However, the co-IP results indicate that PNPase in *Synechocystis* is an enzyme that can recruit either RNase E or RNase J, together with additional proteins.

40 ## Introduction

41 Bacteria are exposed to many environmental changes that require rapid acclimation
42 responses, including the regulation of gene expression. One mechanism is the post-
43 transcriptional regulation of mRNA decay involving the activity of one of the major
44 ribonucleases (RNases), RNase E/G, RNase Y, and/or RNase J. In all bacteria, at
45 least one homolog of these RNases can be found (Laalami, Zig and Putzer 2014; Aït-
46 Bara and Carpousis 2015).

47 RNases are often the scaffold for an mRNA degradation machinery, the degradosome.
48 In *E. coli*, RNase E possesses binding domains in its C-terminal region to recruit the
49 exoribonuclease polyribonucleotide nucleotidyltransferase (PNPase), the RNA
50 helicase RhlB and the glycolytic enzyme enolase (Vanzo *et al.* 1998). In the Gram-
51 positive bacterium *B. subtilis*, the degradosome complex is assembled around RNase
52 Y, which, similarly to the *E.coli* degradosome, interacts with PNPase, the helicase
53 CshA and enzymes involved in glycolysis (Commichau *et al.* 2009; Lehnik-Habrink *et*
54 *al.* 2010; Newman *et al.* 2012).

55 An RNase E-based RNA degradosome exists also in cyanobacteria (Zhang, Hess and
56 Zhang 2022). It was first shown in the filamentous cyanobacterium *Nostoc* (*Anabaena*)
57 sp. PCC 7120 that the noncatalytic region of RNase E recruited PNPase, and that the
58 two proteins interact through a widely conserved nonapeptide within the RNase E C-
59 terminal region (subregion C4) (Zhang *et al.* 2014). Later, the 3' exoribonuclease
60 RNase II was found to be another RNase E-associated ribonuclease in this organism
61 (Zhou *et al.* 2020), and there is strong evidence for further additional interacting
62 proteins, such as the RNA helicase CrhB, enolase (Yan *et al.* 2020), and the

63 conserved protein RebA (Liu *et al.* 2024). RebA is an inhibitor of RNase E catalytic
64 activity and is universally conserved in cyanobacteria (Liu *et al.* 2024).

65 Besides mRNA degradation, the degradosome enzymes play important roles in other
66 biological processes, such as in the control of translation (Redko *et al.* 2013) or the
67 maturation of CRISPR-related transcripts (crRNAs) (Behler *et al.* 2018). The type III-
68 A CRISPR/Cas system of *Staphylococcus epidermidis* relies on the degradosome
69 associated PNPase and RNase J2 to promote crRNA maturation and for efficient
70 clearance of phage-derived nucleic acids (Chou-Zheng and Hatoum-Aslan 2019).

71 In the cyanobacterial model *Synechocystis* sp. PCC 6803 (hereafter *Synechocystis*),
72 three distinct CRISPR/Cas systems were described. These are a type I-D (CRISPR1),
73 a type III-Dv (CRISPR2), and a III-Bv (CRISPR3) system, which are highly expressed
74 under a variety of conditions and active in interference assays (Scholz *et al.* 2013,
75 2019; Kieper *et al.* 2018; McBride *et al.* 2020; Bilger *et al.* 2024; Schwartz *et al.* 2024).
76 While the CRISPR1 and CRISPR2 systems depend on Cas6 endoribonucleases for
77 the maturation of crRNAs (Scholz *et al.* 2013; Reimann *et al.* 2017), no such enzyme
78 is affiliated with the CRISPR3 system. Instead, the CRISPR3 system depends on the
79 major ribonuclease RNase E to process crRNAs in this system. It catalyzes a single
80 cleavage within the repeats, directly generating the 13 and 14 nt long 5' repeat handles
81 (Behler *et al.* 2018). However, the sequences between the spacer ends and the 5'
82 handle of the next following crRNA disappear and also do not accumulate as individual
83 fragments. These observations and the accumulation of mature crRNAs exclusively
84 48 and 42 nt in length suggested the involvement of at least one additional
85 ribonuclease in the maturation of CRISPR3-derived crRNAs (Scholz *et al.* 2013;
86 Behler *et al.* 2018).

87 In addition to RNase E (*slr1129*), RNase J (*slr0551*) is present in *Synechocystis*, a
88 combination that is conserved in cyanobacteria (Laalami and Putzer 2011). RNase E
89 has been analyzed in more depth than RNase J, but it is clear that both enzymes target
90 a wide range of transcripts (Cavaiuolo *et al.* 2020; Hoffmann *et al.* 2021, 2024). Neither
91 the gene encoding RNase E nor the gene for RNase J can be deleted in *Synechocystis*
92 indicating their essentiality. However, *Synechocystis* contains multiple chromosome
93 copies (Zerulla, Ludt and Soppa 2016), making partial gene deletions possible to
94 generate knockdown mutants with a reduced gene copy number. Analysis of such a
95 partial *rnj* deletion (strain δ*rnj*) indicated that the maturation of crRNAs from the
96 CRISPR3 system could involve RNase J (Cavaiuolo *et al.* 2020).

97 RNase J was first discovered in *Bacillus subtilis* (Even *et al.* 2005), but is wide-spread
98 also in other bacteria, in many archaea (Hasenöhrl, Konrat and Bläsi 2011; Levy *et al.*
99 2011; Zheng *et al.* 2017), and also present in plant and algal chloroplasts (Chen, Zou
100 and Zhao 2015; Liponska *et al.* 2018; Hotto, Stern and Schuster 2020). RNase J
101 belongs to the β-CASP protein family within the superfamily of metallo-β-lactamase
102 fold proteins (Callebaut *et al.* 2002), with two beta lactamase domains separated by a
103 β-CASP domain (Condon and Gilet 2011). The enzyme possesses an endonuclease
104 and a unique 5'-3' exonuclease activity (Mathy *et al.* 2007), the latter previously
105 thought to be absent in prokaryotes (Alifano, Bruni and Carlomagno 1994; Deana and
106 Belasco 2005). Despite these insights, RNase J is still less well investigated in
107 comparison to RNase E (Ehretsmann, Carpousis and Krisch 1992; Mackie 2013;
108 Zhang *et al.* 2014; Chao *et al.* 2017; Hoffmann *et al.* 2021, 2024; Liu *et al.* 2024), or
109 RNase Y (Shahbabian *et al.* 2009; Lehnik-Habrink *et al.* 2011; Marincola *et al.* 2012;
110 Scornet *et al.* 2024).

111 Here, we investigated if RNase J is involved in the maturation of pre-crRNA in
112 *Synechocystis* and identified putative cleavage sites. Through co-immunoprecipitation
113 (co-IP) coupled with mass spectrometry we identified RNase J interaction partners,
114 pointing at possible further proteins interacting with RNase J in *Synechocystis.*

115

116 # Methods

117 ## Strains and cultivation

118 *Synechocystis* cultures were grown at 30°C in 50 mL copper-depleted BG11 medium
119 (Rippka *et al.* 1979) supplemented with 20 mM TES (N-[Tris-(hydroxymethyl)-methyl]-
120 2-aminoethane sulfonic acid) under continuous illumination with white light at 30 – 50
121 µmol photons m^{-2} s^{-1} and constant shaking. The cultures were supplied with
122 appropriate antibiotics, namely kanamycin (50 µg/mL) and gentamicin (2 µg/mL) for
123 *Synechocystis* strains carrying pVZ322 (Zinchenko *et al.* 1999) constructs, and
124 kanamycin (100 µg/mL) and spectinomycin (200 µg/mL) for the strains carrying the
125 spectinomycin resistance cassette and a pVZ322 vector. For co-IP assays, four
126 biological replicates of strains overexpressing N- or C-terminally tagged RNase J and
127 GFP controls were cultivated in a high-density cultivation system (HD100 Cultivator
128 from CellDEG GmbH) in 100 mL of fresh water organism (FWO) medium (Migur *et al.*
129 2021) at a starting OD_{750} of 0.9 – 1.0. FWO medium consists of 50 mM $NaNO_3$, 15 mM
130 KNO_3, 2 mM $MgSO_4$, 0.5 mM $CaCl_2$, 0.025 mM H_3BO_3, 0.15 mM $FeCl_3$/Na_2EDTA, 1.6
131 mM KH_2PO_4, 2.4 mM K_2HPO_4, 10 mM $NaHCO_3$, 10 µM $MnCl_2$, 1 µM $ZnSO_4$, 0.1 µM
132 Na_2MoO_4, 0.01 µM $CuSO_4$ and 0.03 µM $CoCl_2$. High CO_2 concentration were delivered
133 from a carbonate buffer (8.29 g K_2CO_3 and 54.06 g $KHCO_3$ in 200 mL deionized water)
134 according to manufactures instructions. Kanamycin and gentamicin were added as

135 described (Migur *et al.* 2021). RNase J or GFP expression was induced with 2 µM of
136 Cu^{2+} or 6 mg/mL of L-rhamnose, according to the expression system, for 24 h before
137 harvesting (final OD_{750} of approximately 25 – 30). An equivalent of 1000 OD of cells
138 were collected by centrifugation (3,200 × g, 10 min, at room temperature). Pellets were
139 stored at -70°C until further processing.

140

141 **Construction of RNase J expression vectors**

142 We constructed two different systems for the expression of 3×FLAG-tagged RNase J.
143 First, we constructed the pVZ322-P_{petE}-*slr0551* vector with and without a C-terminal
144 3×FLAG tag. The *slr0551* native gene and the *petE* gene promoters were amplified
145 from *Synechocystis* genomic DNA using primer pairs RB1/ RB2 and RB3/RB4,
146 respectively. The PCR products were separated on 0.8% agarose gels, visualized with
147 ethidium bromide and correctly-sized fragments were excised and purified with the
148 NucleoSpin Gel and PCR Clean-up kit (Machery-Nagel GmbH), according to
149 manufacturer's instructions. Then, the fragments were ligated by AQUA cloning (Beyer
150 *et al.* 2015) into pUC19 reverse-amplified by PCR with primers RB5/ RB6 and
151 transformed into chemically competent *E. coli* DH5α cells (NEB). After confirming
152 correct insert sequences, P_{petE}-*slr0551* was amplified using primers RB7/ RB8, or
153 primers RB9/ RB10 to generate fragments for the inducible RNase J expression with
154 and without a C-terminally 3×FLAG tag. The fragments were ligated into *Pst*I/*Xba*I-
155 digested pVZ322 via AQUA cloning. The final pVZ322 constructs were introduced into
156 the *Synechocystis* wild type, WT-Spc and δ*rnj* (Cavaiuolo *et al.* 2020) strains by tri-
157 parental mating (Scholz *et al.* 2013). Constructs were verified via PCR and
158 sequencing.

159 To construct plasmid pVZ322-P_{rha}-3×FLAG-*slr0551* for the expression of RNase J with
160 an N-terminal 3×FLAG tag under the control of an rhamnose-inducible promoter (Kelly
161 *et al.* 2018, 2019), primers RB11/ RB12 were used to amplify a 3×*flag-slr0551*
162 fragment. In parallel, the backbone was reverse-amplified from plasmid
163 pUC19P_{rha}YFP3×FLAG (Hemm *et al.* 2024) using primer pair RB13/ RB14 . After gel
164 separation and excision, the two amplicons were treated with FastDigest *Dpn*I
165 (Thermo Fisher Scientific) to eliminate template DNA. The construct was assembled
166 via AQUA cloning (Beyer *et al.* 2015) by transformation into DH5α chemical competent
167 *E. coli* cells (NEB). Correct insertion of the *slr0551* fragment was checked by colony
168 PCR with primer pair RB15/ RB16 using One*Taq* polymerase (NEB) and positive
169 clones were sequenced by IDT (Integrated DNA Technologies, Inc). Correct
170 constructs were selected for PCR with primer pair RB15/ RB16 using PCRBio HiFi
171 polymerase (PCR Biosystems Ltd.) and cloned into *Xmn*I-digested pVZ322s (pVZ322
172 lacking the kanamycin cassette (Kaltenbrunner *et al.* 2023)) by AQUA cloning. The
173 verified construct was then introduced in *Synechocystis* wild type via tri-parental
174 mating (Scholz *et al.* 2013). Correct clones were identified by PCR and verified by
175 sequencing. Primers used in this work are listed in **Supplementary Table S1**.

176

177 **RNA isolation**

178 *Synechocystis* wild type, the strain with spectinomycin cassette integrated into a
179 neutral site (in the *ssl0452-slr0271* intergenic region, strain WT-Spc (Cavaiuolo *et al.*
180 2020)), and δ*rnj* strains with and without pVZ322 constructs for RNase J expression
181 were cultivated in copper depleted BG11 with appropriate antibiotics. When the
182 cultures reached an OD_{750} of approximately 0.5, they were induced with 2 μM $CuSO_4$

183 and collected by vacuum filtration on hydrophilic polyethersulfone filters (Pall Supor®-
184 800, 0.8 µm) at time point 0 (before induction), and 24 and 48 h thereafter. The filter
185 was transferred to a tube containing 1 mL of PGTX (39.6 g phenol, 6.9 g glycerol, 0.1
186 g 8-hydroxyquinoline, 0.58 g EDTA, 0.8 g sodium acetate, 9.5 g guanidine thiocyanate,
187 4.6 g guanidine hydrochloride) (Pinto *et al.* 2009), snap frozen in liquid nitrogen and
188 stored at - 80°C. For the RNA extraction, the samples were incubated for 15 min at
189 65°C, 1 mL of chloroform/isoamyl alcohol (IAA) (24:1) was added and the samples
190 were incubated for 10 min at room temperature. Phase separation was performed by
191 centrifugation for 5 min at 3,270 × g at room temperature. The upper aqueous phase
192 was transferred to a new tube, mixed with one volume of chloroform/IAA (24:1) and
193 centrifuged again. The aqueous phase was transferred to a new tube, mixed with one
194 volume of isopropanol and precipitated overnight at -20°C. The precipitated RNA was
195 pelleted by centrifugation (13,000 × g, 30 min, 4°C). The pellet was washed with 700
196 µL of 70% ethanol (13,000 × g, 10 min, 4°C), air-dried and resuspended in 20 – 40 µL
197 of nuclease-free water. RNA concentration was determined using a
198 spectrophotometer (NanoDrop ND-1000, Peqlab). The RNA quality was assessed by
199 loading 10 µg of RNA on an 8 M urea, 10% polyacrylamide (PAA)-Tris-Borate-EDTA
200 (TBE) gel.

201

202 **Northern analysis**

203 Northern hybridization and analysis was performed as described previously (Bilger *et*
204 *al.* 2024). Primers RB17 and RB18 were used to generate the template for probe
205 generation used in the hybridization of CRISPR3 crRNA, covering the region from

206 spacer 1 to spacer 4. Desoxyoligonucleotide RB19 was used for quantification of the
207 5S RNA.

208

209 **Primer extension assay**

210 Primer extension was performed as described previously (Behler *et al.* 2018) using
211 the primers RB20 and RB21 (called PrimerExt_Ladder_fwd and PrimerExt_S3_rev in
212 Behler *et al.* (2018)) to target the same region in the CRISPR3 pre-crRNA transcript,
213 and using RNA from *Synechocystis* WT-Spc or δ*rnj* strains, carrying different pVZ322
214 constructs. The cells were harvest 24 h post-induction and RNA was isolated as
215 described above.

216

217 **RNase J co-IP and proteomic sample preparation**:

218 Cell pellets from CellDEG cultures were resuspended in 1.5 mL FLAG buffer (50 mM
219 Hepes-NaOH pH 7.5 mM $MgCl_2$, 25 mM $CaCl_2$, 150 mM NaCL, 10% glycerol, 0.1%
220 Tween-20 and cOmplete Protease inhibitor (Roche)) and split in three screw-cap tubes
221 containing 250 µL glass beads (Ø 0.1-0.25 mm, Retsch). The cells were lysed using
222 a prechilled Precellys homogenizer (Bertin Technologies). To remove cell debris and
223 glass beads, the samples were centrifuged at 13,000 × g for 30 min at 4°C. The
224 supernatant (soluble crude extract) was incubated with 100 µL of packed anti-FLAG®
225 M2 magnetic beads (Sigma Aldrich), for 2 hours at 4°C under gentle rotation. The
226 beads were washed 6 times with 2 mL of FLAG-buffer using DynaMag™-2 magnetic
227 rack (Thermo Fisher). The attached proteins were eluted with 250 µL TBS containing

228 0.4 mg/mL FLAG peptide as competitor. The samples were incubated for 30 min at
229 4°C under gentle rotation. The supernatant was taken as elution fraction.

230 For MS analysis, 10 µg of protein per sample was prepared by adding 1% SDS and 5
231 mM DTT, followed by an incubation at 60°C for 30 min with shaking at 1,000 rpm. in a
232 ThermoMixer® (Eppendorf). Reduced disulfides were alkylated by adding 0.1 vol of 2-
233 chloroacetamide (200 mM) and incubation for 15 min at 37°C and shaking. The
234 alkylation reaction was quenched by adding 5 mM of DTT. The protein clean-up and
235 digestion was performed following the SP3 protocol (Hughes *et al.* 2019). To each
236 sample, 100 µg of a 1:1 mixture of Sera-Mag SpeedBeads suspension (prepared to a
237 50 µg/µL, GE Healthcare®, cat. No. 45152105050250 and 65152105050250) was
238 added. To induce binding of the proteins to the beads, 4 vol of 100% ethanol were
239 added and incubated in a ThermoMixer® at 24°C for 5 min at 1,000 rpm. Tubes were
240 placed in a magnetic rack and the beads were washed 3 times with 180 µL of 80%
241 ethanol. Beads were resuspended in 75 µl of 100 mM ammonium bicarbonate, pH 8
242 containing 0.24 µg of sequencing grade, modified trypsin (Promega), sonicated for 30
243 s in a water bath to disaggregate the beads and incubated for 18 h at 37°C in a
244 ThermoMixer® at 1,000 rpm. After digestion, the samples were centrifuged at 20,000
245 × g for 1 min at RT. The tubes were placed in the magnetic rack and the supernatant,
246 containing the digested proteins, was transferred to a new tube. Samples were
247 acidified by adding formic acid to a final concentration of approximately 2% to obtain
248 a pH < 3. Next, AttractSPE Tips RPS T1 200 µL (Affinisep) were equilibrated with 50
249 µL methanol centrifuged for 2 min at 1,000 × g, followed by the addition of 50 µL 0.5%
250 acetic acid and another centrifugation. The acidified samples were loaded onto the
251 equilibrated tips and centrifuged. Samples were washed with 30 µL and 60 µL of 0.1%
252 formic acid and 80% acetonitrile. Samples were eluted with 65 µL of freshly prepared

253 5% ammonium hydroxide and 60% acetonitrile in water. Peptides were eluted by
254 centrifugation for 3 min at 500 × g into glass vials. The elution was dried in SpeedVac
255 set at 30°C and stored at - 20°C.

256

257 **Liquid chromatography and electrospray MS**

258 For LC-MS analysis, an UltiMate™ 3000 RSLCnano system was online coupled to an
259 Exploris 480 mass spectrometer (both Thermo Fisher Scientific, Dreieich, Germany).
260 The peptide mixture was washed and preconcentrated on a µPAC™ C18 trapping
261 column (PharmaFluidics) with a flow rate of 10 µL/min and peptides were separated
262 on a µPAC™ C18 pillar array column (50 cm bed length, PharmaFluidics) using a
263 binary buffer system consisting of A (0.1% formic acid) and B (86% acetonitrile, 0.1%
264 formic acid). With a flow rate of 0.5 µL/min peptides were eluted applying an isocratic
265 gradient from 1% to 4% B in 2 min, 4% to 25% B in 24 min, 25% to 44% B in 12 min,
266 44% to 90% in 2 min, and 90% B for 4 min. For electrospray ionization of peptides, a
267 Nanospray Flex ion source (Thermo Fisher Scientific) with a liquid junction PST-HV-
268 NFU (MS Wil, The Netherlands) and a fused silica emitter (20 µm inner diameter, 360
269 µm outer diameter, MicroOmics Technologies LLC) with a source voltage of +1,800 V
270 and an ion transfer tube temperature of 275°C was used. Cycles of data-independent
271 acquisition (DIA) consisted of: one overview spectrum (RF lens of 40%, normalized
272 AGC target of 300%, maximum injection time of 45 ms, *m/z* range of 350 to 1,400,
273 resolution of 120,000) recorded in profile mode followed by MS2 fragment spectra (RF
274 lens of 50%, normalized AGC target of 1000%, maximum injection time of 54 ms)
275 generated sequentially by higher-energy collision-induced dissociation (HCD) at a
276 normalized energy of 28% in a precursor *m/z* range from 361 to 450 in 6 windows of

277 14 *m/z* isolation width, in a precursor *m/z* range from 450 to 800 in 50 windows of 7
278 *m/z* isolation width and in a precursor *m/z* range from 800 to 1,100 in 21 windows of
279 14 *m/z* isolation width, overlapping by 1 *m/z* and recorded at a resolution of 30,000 in
280 profile mode.

281

282 **MS data analysis**

283 MS raw data were converted to mzML format using the ProteoWizard software,
284 version 3.0.21229 (Chambers *et al.* 2012). For protein and peptide identification and
285 quantification a library free search was performed using DIA-NN version 1.8.1
286 (Demichev *et al.* 2020) against the organism-specific Uniprot database (release
287 2023_03, *Synechocystis* sp. strain PCC 6803, taxid 1148), complemented with the
288 sequences of RNase J, 3xFLAG and GFP. Trypsin was set as protease with 2 allowed
289 missed cleavages. Carbamidomethylation of cysteine was selected as fixed
290 modification, N-terminal excision of methionine and oxidation of methionine were
291 selected as variable modifications with a maximum number of 2. For precursor ion
292 generation, peptides ranging from 7 to 35 amino acids, precursor charge from 2 to 4,
293 precursor *m/z* range from 361 to 1,100 and fragment ion *m/z* range from 200 to 1,200
294 were used. Further parameters were: match between runs, unrelated runs, search in
295 double-pass mode, deactivated heuristic protein inference, robust LC quantification
296 and RT-dependent cross-run normalisation. The protein group quantities output file
297 from DIA-NN was used and all proteins with non-zero label-free quantification (LFQ)
298 intensities in 3 out of 4 replicates in both groups were selected for further analysis.
299 Missing values were imputed by sequential imputation using the R package
300 impSeqRob (Verboven, Branden and Goos 2007). For differential abundance

301 analysis, $\log_{10}$ transformed LFQ intensities were subjected to a moderated t-test using
302 the R package limma (Ritchie *et al.* 2015) with correction of p-values for multiple
303 testing using Benjamini and Hochberg's method.

304

305 ## Results

306 **Evidence that RNase J is involved in CRISPR3 crRNA maturation**

307 We first tested the possible effects of RNase J on synthetic RNA substrates *in vitro.*
308 We cloned and expressed histidine-tagged recombinant RNase J as described
309 (Cavaiuolo *et al.* 2020). Purified RNase J was incubated with synthetic
310 oligoribonucleotide RB27 corresponding to the CRISPR3 spacer 2-repeat sequence
311 (substrate, 72 nt). Several weak bands were observed already in the absence of added
312 enzyme indicating slight degradation of the substrate (background). However, a few
313 bands clearly appeared or were increased in intensity upon addition of RNase J.
314 Especially, the more prominent signal at 35 nt (**Fig. 1A**, lane 2), consistent with the
315 primary cleavage at the end of the spacer as inferred from the analysis of primer
316 extension products (**Fig. 2**), followed by exonucleolytic removal of single nucleotides
317 close to the 5´ end of the repeat, as this would yield precisely a 35 nt fragment. Thus,
318 RNase J may have processed the synthetic RNA via its 5´ exonuclease and
319 endonuclease activities combined.

320 The same experiment performed with purified RNase E provided a different cleavage
321 pattern (**Fig. 1A**, lane 3). A prominent appearing band likely is the substrate after 13
322 nt were cleaved off from the 3' end. When incubating the RNA with both ribonucleases,
323 we obtained a cleavage pattern corresponding to the two single digestions combined

324 (lane 4). Because the appearance of multiple bands complicates the interpretation, we
325 then performed analogous experiments with a single synthetic CRISPR3 repeat
326 sequence with a single additional adenosine at the 5´ end yielding a 37 nt substrate.
327 Incubation with RNase E alone resulted in one major band and a minor band one nt
328 shorter (**Fig. 1A**, lane 7). These fragments match previous observations made in *in*
329 *vitro* assays using synthetic CRISPR3 repeat sequences as substrate (Behler *et al.*
330 2018) and release the unusually long, 13 and 14 nt long 5' handles observed *in vivo*
331 (Scholz *et al.* 2013). Incubation with RNase J alone resulted in single major band as
332 well (**Fig. 1A**, lane 6), with a size difference of 2 nt compared to the digestion with
333 RNase E (**Fig. 1A**, lanes 6 and 7). The RNase J cleavage site thus must be close to
334 the processing site used by RNase E to generate the 5´ handle of the CRISPR3 crRNA
335 (**Fig. 1B**). Alternatively, RNase J cleaved the same site as RNase E as
336 endoribonuclease, followed by by exonucleolytic removal of 2 nt until reaching the
337 repeat stem loop blocking further processing (**Fig. 1B**).

338 The absence of a ladder-like pattern suggested that primarily the endonuclease
339 activity of RNase J was active. When mixing both enzymes, we obtained a cleavage
340 pattern qualitatively corresponding to the two single digestions combined, but
341 quantitatively, the RNase J-assigned signal was weaker (**Fig. 1A**, lane 8). This result
342 matches the observation that *in vivo* RNase E is the dominating and rate-limiting
343 enzyme in processing the CRISPR repeat (Behler *et al.* 2018). The *in vitro* cleavage
344 data in **Fig. 1** provide critical evidence that RNase J processes CRISPR3 RNA
345 precursors.

346

347

348 **RNase J expression influences processing of crRNA intermediates *in vivo***

349 To determine whether RNase J affects the maturation of CRISPR3 crRNA *in vivo*,
350 primer extension analysis was performed to map possible processing differences
351 between the strains overexpressing tagged and untagged RNase J *in vivo*. Therefore,
352 we cloned the *slr0551* gene encoding RNase J into the pVZ322 vector under the
353 control of the copper-inducible *petE* promoter, P_{petE} (Zhang *et al.* 1992). We designed
354 two different constructs: one expressing the unmodified RNase J protein, and one
355 expressing a version with a 3×FLAG sequence fused to its C-terminal end. The
356 constructed plasmids were conjugated into *Synechocystis* strain PCC-M (Trautmann
357 *et al.* 2012) via tri-parental mating (Scholz *et al.* 2013). In addition, we included the
358 *Synechocystis* δ*rnj* strain with a reduction in the number of *rnj* loci per cell (partial gene
359 deletion) (Cavaiuolo *et al.* 2020), in which we overexpressed C-terminally tagged, or
360 untagged RNase J. The *rnj* overexpression in *Synechocystis* WT-spc and δ*rnj*-spc
361 strains carrying pVZ322-P_{petE}-*rnj* compared to the control strains with the empty
362 pVZ322 vector as control was verified by northern hybridization (**Supplemental Fig.**
363 **S1**). Because the partial deletion of *rnj* gene copies by insertion of a streptomycin
364 resistance gene in the *Synechocystis* δ*rnj* strain depends on the presence of
365 streptomycin, we used as background for all engineered strains in this experiment not
366 the wild type, but strain WT-Spc, with a spectinomycin cassette integrated into a
367 neutral site within the *ssl0452-slr0271* intergenic region (Cavaiuolo *et al.* 2020). A
368 strain carrying the empty pVZ322 vector was used as control. The cells were cultivated
369 until reaching an OD_{750} of 0.8 and cells were collected 24 h after RNase J expression
370 was induced. Primer extension was performed on 2 µg of total RNA using the same
371 primer previously used to analyze the involvement of RNase E in CRISPR3 maturation
372 (Behler *et al.* 2018). The result is shown in **Fig. 2**. The WT-Spc control strain yielded

373 an identical pattern to previous primer extensions obtained with the *Synechocystis* wild
374 type (Behler *et al.* 2018), indicating that the integrated resistance cassette had no
375 effect on crRNA processing. Moreover, the two strains overexpressing RNase J or
376 RNase J-3×FLAG showed identical patterns to the WT-Spc strain. However, two
377 differences were apparent in the δ*rnj* strain, harboring only the empty vector. In this
378 strain, one additional band and one band with increased intensity were observed (**Fig.**
379 **2**, arrows). While the lower band (arrow 1) was weaker, but present also in the other
380 lanes, the upper band (arrow 2) was unique to the δ*rnj* strain (**Fig. 2**). Because in this
381 strain the RNase J level is the lowest, this observation indicated that

382 a) the reduced level of RNase J in the δ*rnj* strain impacted the processing of the
383 CRISPR3 crRNA maturation and

384 b) this effect was reversed when overexpressing recombinant RNase J from a plasmid.

385 Using the sequence ladder on the left, we identified the corresponding sequences of
386 the observed bands. The 3' ends of the two fragments were located close, 1 and 3 nt,
387 to the 3' ends of spacer 2 (S2) of the CRISPR3 array (**Fig. 2B,** arrows 1 and 2). As
388 these two fragments accumulated in the cell, we conclude that the depletion in RNase
389 J caused a bottleneck in the processing of the crRNA.

390 Previous work identified the first cleavage site of the CRISPR transcript is located at
391 the end of the spacer, at exactly these positions, 1 to 3 nt from the first nt in the repeat
392 (**Fig. 2B**, arrows), leading to the 72 nt intermediate (see Fig. 3 in Scholz *et al.* (2013)).
393 Thus, the corresponding transcript was a substrate for RNase J activity, which was
394 limiting in this strain. As RNase J from *Synechocystis* possesses 5´ exonuclease
395 activity (Cavaiuolo *et al.* 2020), it may then remove 2 to 4 further nucleotides from the
396 5´ end until reaching the stem-loop structure beginning at nt 2 of the repeat. That

397 structure then is recognized by RNase E in a further processing step, which generates
398 the crRNA 5´ handle (Behler *et al.* 2018).

399 Northern analyses were used to validate possible effects of RNase J overexpression
400 on the accumulation of CRISPR3 processing intermediates. *Synechocystis* wild type
401 served as control. Samples were harvested over a time course of 24, 72 and 144 h
402 post induction and RNA was isolated for each strain. The impact of ribonuclease J
403 overexpression on CRISPR3 crRNA maturation was analyzed using a radioactively
404 labeled single-stranded RNA probe spanning the CRISPR3 spacers 1 to 4. The
405 resulting complex pattern of mature crRNAs and processing intermediates in the wild
406 type was fully consistent with previous analyses (Scholz *et al.* 2013; Behler *et al.*
407 2018). The mature crRNA forms of 48 and 42 nt were among the strongest signals
408 (**Fig. 3**). Another strong signal was obtained for the 72 nt, 144 nt and 216 nt long
409 processing intermediates consisting of single, double and triple repeat-spacer units.
410 Moreover, the previously reported 6 nt-periodicity (Behler *et al.* 2018) was visible in
411 the form of the double bands for the mature crRNAs and all processing intermediates.
412 At time point T0, prior to induction, we expected that the wild type and the two
413 overexpression strains should show quantitatively and qualitatively similar signals.
414 While all strains did show similar patterns, most band intensities were stronger in the
415 strain carrying the construct for the overexpression of the untagged enzyme (*rnj* OE).
416 Especially striking was the difference for the smaller RNA fragments, the 144 nt and
417 shorter processing intermediates, and the mature crRNAs. This observation may be
418 explained by the leakiness of the P_{petE} promoter. Furthermore, we noticed a slight
419 reduction in the intensities of the signals between 100 and 250 nt in the strain encoding
420 the tagged enzyme (*rnj-3xF* OE) (**Fig. 3**). This difference in activity between the tagged

421 and untagged RNase J became more pronounced during the later times of the time
422 course.

423 The most striking difference was seen in the disappearance of a ~70 nt band (marked
424 by a black arrow in **Fig. 3**) in the strain overexpressing the tagged enzyme after
425 induction. The size of the band slightly below the main signal for the single repeat-
426 spacer unit of 72 nt indicates that it is an crRNA maturation intermediate 2 or 3 nt
427 shorter. The increased signal intensities in the strain overexpressing untagged RNase
428 J confirmed that RNase J is involved in the maturation of crRNA from the subtype III-
429 Bv CRISPR system in *Synechocystis*. Furthermore, the tagging of RNase J at its C-
430 terminal end may have enhanced its exoribonuclease activity, explaining the overall
431 lower crRNA signal intensities in this strain and especially the disappearance of the
432 signal at ~70 nt at the T24, T72 and T144 time points in the strain overexpressing the
433 tagged enzyme. Previous observations indicated an enhanced 5' exoribonuclease
434 activity for C-terminally poly-histidine-tagged RNase J1 in *Bacillus subtilis* (Laalami
435 and Putzer 2011), which would be consistent with the observations made here for the
436 C-terminally tagged RNase J.

437

438 **Characterization of proteins interacting with RNase J**

439 We next sought to identify potential interaction partners of RNase J. Co-IP
440 experiments were performed with *Synechocystis* strains expressing RNase J either N-
441 or C-terminally tagged with the 3×FLAG epitope, and with GFP-expressing strains as
442 controls (plasmids pVZ322-P_{rha}-*3×FLAG-slr0551*, pVZ322-P_{rha}-*gfp-3×FLAG*, pVZ322-
443 P_{petE}-*slr0551-3×FLAG,* or pVZ322-P_{petE}-*gfp-3×FLAG*). The strains were cultivated in
444 quadruplicates in high density cultivation systems (CellDEG GmbH) until an OD_{750} of

445 approximately 9–12 was reached, and protein expression was induced for 24 h before
446 harvesting the cells, with a final OD_{750} of approximately 25–30. Triple-FLAG tagged
447 proteins were purified with M2 anti-FLAG magnetic beads and analyzed by SDS-
448 PAGE (**Supplemental Fig. S2 and S3**). Potential interaction partners were identified
449 by mass spectrometry. In the entire dataset, a total of 2,625 proteins was identified,
450 corresponding to ~71.5% of the total proteome. The list of proteins identified for each
451 replicate is detailed in **Supplemental Table S2**.

452 In order to identify potential interaction partners, a $\log_2$FC threshold of +1.5 (p value ≤
453 0.05) was established to select proteins which were at least 2.8-fold enriched in the
454 RNase J overexpression strains with respect to the GFP expressing control strains.
455 With this parameter, 20 proteins were identified for the N-terminal tagged (NTT)
456 RNase J and 36 proteins for the C-terminal FLAG-tagged (CTT) RNase J. In both
457 cases, RNase J, used as bait, showed the highest respective enrichment ($\log_2$FC of
458 +10.26 and +12.13). In addition to RNase J, eight enriched proteins were shared
459 between the two co-IPs with the differentially tagged RNase J variants.

460 A gene ontology analysis was conducted to categorize the identified proteins
461 according to their PANTHER protein class (Thomas *et al.* 2022). Approximately one
462 third of the detected proteins were not assigned to a PANTHER category (35.0% for
463 NTT and 35.3% for CTT RNase J). In both batches, the second most enriched
464 prominent group (after unclassified) was that of metabolite interconversion enzymes
465 (35.00% in NTT and 14.70% in CTT RNase J). In CTT, proteins were assigned to DNA
466 metabolism (11.80%), protein modifying enzymes (8.80%) and translational proteins
467 (5.90%) which were not found in the NTT batch. Chaperone proteins represent 10.0%
468 in the NTT batch and 5.9% in the CTT batch (**Supplementary Table S3**).

469 The calculated log_2FC data were plotted over the adjusted p values in the form of a
470 volcano plot (**Fig. 4**). Among the nine proteins shared between the co-IPs with the two
471 differentially tagged RNase J variants, PNPase stood out with log_2FC enrichment
472 factors of +4.67 and +5.96 (**Table 1**). Five of the other proteins that were found
473 consistently enriched with both NTT and CTT RNase J have regulatory functions.
474 These were EbsA, a factor essential for biofilm self-suppression that interacts with Hfq
475 and PilB (Yegorov *et al.* 2021), the PatA family regulator of phototaxis PisG (Yoshihara
476 *et al.* 2000), the RuBisCO transcriptional regulator (Bolay *et al.* 2022), Sll0245, a
477 possible homolog the ribosome-binding ATPase YchF (Tomar, Kumar and Prakash
478 2011), and Sll0086, annotated as a one-domain ArsA-like protein, although
479 experimental analyses indicated that it is not involved in arsenic or antimony
480 resistance (López-Maury, Florencio and Reyes 2003). Further consistently enriched
481 proteins were Slr0244 containing a universal stress protein A (UspA) domain, and
482 Slr0552, an unknown protein encoded by a gene directly downstream of *rnj* (**Table 1**).

483

484 **PNPase is not involved in CRISPR3 crRNA maturation**

485 PNPase was the most highly enriched ribonuclease in the RNase J co-IP (**Fig. 4A, B**).
486 Moreover, the PNPase in *Synechocystis* forms a complex with RNase E (Zhang *et al.*
487 2014), therefore it was considered as another candidate for participation in the
488 CRISPR3 crRNA maturation in *Synechocystis*. We expressed PNPase as a
489 recombinant protein in *E. coli*, purified and tested its activity in *in vitro* cleavage assays.
490 The samples with the successive addition of PNPase or RNase E showed the 22 and
491 23 nt cleavage products expected for cleavage by RNase E and remaining substrate
492 (Behler *et al.* 2018). In all samples in which PNPase was added first, the intensity of

493 the 36 nt substrate was lowered indicating the rapid degradation of the substrate (**Fig.**
494 **5**). Moreover, these samples showed a single nt ladder although of very low intensity,
495 directly below the substrate. When RNase E was added first, all samples showed a
496 stronger intensity of the 22 and the 23 nt products, likely because the entire substrate
497 amount had been available for the cleavage by RNase E or because RNase E, when
498 bound to the RNA, protects the substrate from the 3´exonuclease activity of PNPase.
499 The other way around, when PNPase was added first, a part of the substrate was
500 degraded first and only the rest of the substrate was available for the cleavage by
501 RNase E (**Fig. 5**).

502 Samples incubated only with PNPase, irrespectively of incubation times and whether
503 1 or 3 pmol enzyme were used, showed a single nt ladder, although more substrate
504 was degraded when more PNPase was used (**Fig. 5**, lanes to the right). We noticed
505 that the ladder pattern was restricted to the 17 to 36 nt size range. This limitation was
506 not an effect of the used gel conditions as the alkaline hydrolysis of the same substrate
507 showed the ladder extending much further down. However, this result fits to the
508 secondary structure of the CRISPR repeat used as substrate: it consists of a single
509 stem loop from position 2 to 18, while the sequence from nt 19 to 36 is single-stranded
510 (Behler *et al.* 2018). Hence, this result is consistent with a strong 3' exonuclease
511 activity of the *Synechocystis* PNPase that stopped once the stem loop was reached.

512

513 # Discussion

514 **RNase J is involved in the CRISPR3 crRNA maturation**

515 In the type III-Bv CRISPR3 system of *Synechocystis*, RNase E replaces the lacking
516 Cas6 activity in the maturation of the pre-crRNA (Behler *et al.* 2018). Although RNase
517 E is responsible for a major processing step, it has been suggested that additional
518 ribonucleases are involved. While RNase E cleaves within the CRISPR3 repeat RNA,
519 directly generating the characteristic 13 nt and 14 nt 5′ repeat handles (Behler *et al.*
520 2018), it does not generate the 3' ends of the mature crRNAs. Based on the analysis
521 of mapped transcriptome reads, we previously characterized CRISPR3 crRNA
522 maturation as a 2-step process (Scholz *et al.* 2013). This analysis revealed that the
523 first cleavage site is located in the spacer and not in the repeat. This conclusion was
524 supported by the observation that the 72 nt processing intermediate spans across the
525 cleavage site within the repeats and ends at the cleavage site in the spacer (Scholz *et*
526 *al.* 2013).

527 Here, we show that overexpression of RNase J correlates with an increased
528 abundance of the ~72 nt fragment, which represents a single repeat-spacer unit, of
529 other intermediates, and of the 48 nt and 42 nt mature crRNAs (**Fig. 1**). The results of
530 the primer extensions clearly identified two 5' ends that were enriched in the δ*rnj* strain
531 with decreased RNase J activity (**Fig. 2**). These results, in conjunction with the results
532 of Behler et al. (2018), suggest that RNase J mediates 5' exonucleolysis immediately
533 after the first cleavage, an endonucleolytic cleavage close to the spacer 3' ends. After
534 this, RNase E releases the mature crRNA 5' ends including the 13 or 14 nt 5′ repeat
535 handle (the 1 nt size difference in the length of the repeat handle likely results from
536 ambiguity in the substrate cleavage by RNase E itself (Behler *et al.* 2018)).

537 Looking for proteins that interact with RNase J could reveal factors that potentially
538 influence the activity or substrate recognition of RNase J, or act as an additional
539 nuclease involved in further 3' processing. Such processing is required as two mature
540 crRNA forms accumulate *in vivo*, 42 and 48 nt in length and only the latter results from
541 the combined action of RNase E and J. Therefore, we searched for proteins possibly
542 interacting with RNase J. This search identified PNPase as an enzyme strongly co-
543 enriched with RNase J (**Fig. 4**). PNPase is participating in crRNA maturation in *Listeria*
544 *monocytogenes* (Sesto *et al.* 2014) and *Bacillus subtilis* (Chou-Zheng and Hatoum-
545 Aslan 2019). In the Type III-A CRISPR–Cas system of *Staphylococcus epidermidis*,
546 Csm5 was found to interact and stimulate PNPase activity (Walker *et al.* 2017). These
547 findings prompted us to overexpress and test PNPase from *Synechocystis*. While the
548 characterization of *Synechocystis* PNPase in an *in vitro* assay demonstrated a strong
549 3' exonuclease activity (**Fig. 5**), we found no evidence supporting its involvement in
550 CRISPR3 maturation, at least *in vitro*. In the elution of the CTT RNase J, the
551 bifunctional nuclease domain protein Sll1142 was identified. Homologs of this protein
552 are conserved in cyanobacteria, and related proteins exist in many other bacteria and
553 plants. A homolog in *Oryza minuta* was reported to possess bifunctional RNase and
554 DNase activities *in vitro* (You *et al.* 2010). However, whether Sll1142 has any CRISPR-
555 related function remains to be elucidated.

556 The here described involvement of RNase J in the maturation of CRISPR3 crRNAs
557 adds further evidence on the connection between degradosome components and the
558 type III CRISPR-Cas machinery (Behler *et al.* 2018; Chou-Zheng and Hatoum-Aslan
559 2019; Bilger *et al.* 2024). Our current model for CRISPR3 crRNA maturation is shown
560 in **Fig. 6**.

561

562 **Co-IP analysis indicates the existence of a degradosome in *Synechocystis***
563 **involving RNase J**

564 We identified several potential interaction partners for the bifunctional endo- and
565 exoribonuclease RNase J in *Synechocystis*. We conducted a co-IP experiment with
566 N- or C-terminal 3×FLAG-tagged RNase J. The results revealed a significant
567 difference between the two pull-downs. In addition to RNase J, 35 enriched proteins
568 were identified for the CTT RNase J and 19 proteins for the NTT RNase J. Notably,
569 only eight proteins were enriched in both co-IPs (**Table 1**). This discrepancy suggests
570 that the presence and position of the 3×FLAG tag on RNase J was a relevant factor.
571 The detection of five proteins with regulatory functions, EbsA, PisG, Sll0086, RbcR
572 and YchF, that were consistently enriched in the co-IP with RNase J suggests an
573 involvement of RNase J in regulatory responses that require ribonucleases to degrade
574 transcripts that are no longer required.

575 Intriguingly, the most enriched protein together with RNase J was PNPase. The
576 composition of RNA degradosomes varies considerably between different species
577 (Tejada-Arranz, de Crecy-Lagard and de Reuse 2020; Zhang, Hess and Zhang 2022),
578 but they share the presence of at least one major RNase (either RNase E, J or Y) and
579 an RNA helicase (Tejada-Arranz, de Crecy-Lagard and de Reuse 2020). In the
580 cyanobacteria *Nostoc* (*Anabaena*) sp. PCC 7120 and *Synechocystis*, RNase E forms
581 a complex with PNPase, wherein the latter recognizes a conserved nonapeptide
582 RRRRRRSSA at the end of RNase E (RRRRRSSA in *Synechocystis*) (Zhang *et al.*
583 2014). In our study, RNase E was not enriched in comparison to the GFP control.
584 However, PNPase was the most enriched protein in both, CTT and NTT RNase J co-
585 IPs. These data suggest that PNPase can interact not only with RNase E, but also
586 with RNase J. RNase J carries a conserved arginine-rich motif close to its C terminus

587 (RRSRKRS in *Synechocystis*), as is found in RNase E. Structure prediction using
588 Alphafold 3 (Abramson *et al.* 2024) rendered five structures, four of which showed a
589 potential interaction between the arginine-rich motif of RNase J and PNPase, although
590 with only moderate pTM and iPTM support scores of 0.52 and 0.51, respectively
591 (**Supplemental Fig. S4**). The residues that possibly bind PNPase to the C-terminal
592 domain (CTD) of RNase J were compared with previously identified interaction sites
593 of PNPase and RNase E in *E. coli* (Durán-Figueroa *et al.* 2006). The residues from
594 our prediction were all located within the interaction domain of PNPase
595 (**Supplemental Fig. S5**), indicating that the same region might be responsible for the
596 interaction, though *E. coli* RNase E does not possess the arginine-rich motif from
597 *Synechocystis* RNase E or RNase J. In *Synechocystis,* PNPase may form a complex
598 with either RNase E or RNase J, but it is not possible to conclude which interaction is
599 favored under standard growth conditions, as the overexpression of RNase J in the
600 cell may have favored the binding of PNPase to ribonuclease J. In *M. tuberculosis*,
601 PNPase, RNase E, RNase J, and RNA helicase RhlE were predicted to interact
602 (Płociński *et al.* 2019). Similarly, in *Bacillus subtilis* RNase Y, PNPase, the helicase
603 CshA and the glycolytic enzymes enolase and PfkA interact (Lehnik-Habrink *et al.*
604 2010). These studies have shown that the composition of the enzyme complexes that
605 degrade RNA and the interactions among the involved enzymes are also rapidly
606 changing (Cascante-Estepa, Gunka and Stülke 2016). In analogy, it cannot be
607 excluded that *Synechocystis* RNase E and RNase J may interact together, or
608 separately with PNPase, or other factors to degrade RNA.

609 While we identified RNase J as part of the machinery enabling the maturation of
610 CRISPR3 crRNA in the absence of Cas6 enzymes, we were unable to identify
611 enriched Cas proteins from the CRISPR3 effector complex. This indicates that RNase

612 J does not perform an interaction with the effector complex, or that the crRNA is loaded
613 into the Cmr effector complex at a later stage.

614 One uncharacterized protein that was enriched in both RNase J co-IPs was Slr0552.
615 This is of interest because RNase J (Slr0551) and Slr0552 are encoded by two genes
616 in the same operon. A BlastP search revealed that homologs exist in cyanobacteria;
617 however, none of the homologs has been characterized so far.**.** Synteny analysis of
618 the genomic organization of *rnj* and *slr0552* homologs show a conserved synteny in
619 the *Synechocystis* genus and also in more distantly related cyanobacteria like
620 *Gloeothece* and *Crocosphaera* (**Supplementary Fig. S6)**. Structural analysis with
621 Foldseek and HHpred did not return any reliable results. Therefore, the function of
622 Slr0552 and its relationship to RNase J remains a subject for future investigation.

623

624 ## Data availability

625 MS proteomics data have been deposited to the ProteomeXchange Consortium via
626 the PRIDE partner repository (Perez-Riverol *et al.* 2025) and are available through the
627 identifier PXD060866.

628

629 ## Funding

630 This work was supported by the German Research Foundation priority program
631 SPP2141 (grant HE 2544/14-2 to WRH).

632

Acknowledgments

We thank Viktoria Reimann, Freiburg, for the 5S rRNA hybridization in **Fig. 3** and Juliane Behler, Freiburg, for helpful comments in an early phase of the project.

Author contributions

WRH designed the project and secured funding. FD, BK and PH carried out MS-based proteomic analyses. TB carried out all PNPase-related experiments, HL contributed to the co-IP analyses, all other experiments were performed by RB. Data were analyzed by RB, FD, HP and WRH; RB and WRH wrote the manuscript with input from all authors.

644 **References**

645 Abramson J, Adler J, Dunger J *et al.* Accurate structure prediction of biomolecular
646 interactions with AlphaFold 3. *Nature* 2024;**630**:493–500.
647 Aït-Bara S, Carpousis AJ. RNA degradosomes in bacteria and chloroplasts:
648 classification, distribution and evolution of RNase E homologs. *Mol Microbiol*
649 2015;**97**:1021–135.
650 Alifano P, Bruni CB, Carlomagno MS. Control of mRNA processing and decay in
651 prokaryotes. *Genetica* 1994;**94**:157–72.
652 Behler J, Sharma K, Reimann V *et al.* The host-encoded RNase E endonuclease as
653 the crRNA maturation enzyme in a CRISPR–Cas subtype III-Bv system. *Nat*
654 *Microbiol* 2018;**3**:367–77.
655 Beyer HM, Gonschorek P, Samodelov SL *et al.* AQUA cloning: a versatile and simple
656 enzyme-free cloning approach. *PLOS ONE* 2015;**10**:e0137652.
657 Bilger R, Migur A, Wulf A *et al.* A type III-Dv CRISPR-Cas system is controlled by the
658 transcription factor RpaB and interacts with the DEAD-box RNA helicase CrhR.
659 *Cell Rep* 2024;**43**, DOI: 10.1016/j.celrep.2024.114485.
660 Bolay P, Schlüter S, Grimm S *et al.* The transcriptional regulator RbcR controls
661 ribulose-1,5-bisphosphate carboxylase/oxygenase (RuBisCO) genes in the
662 cyanobacterium *Synechocystis* sp. PCC 6803. *New Phytol* 2022;**235**:432–45.
663 Callebaut I, Moshous D, Mornon J *et al.* Metallo-β-lactamase fold within nucleic acids
664 processing enzymes: the β-CASP family. *Nucleic Acids Res* 2002;**30**:3592–
665 601.
666 Cascante-Estepa N, Gunka K, Stülke J. Localization of components of the RNA-
667 degrading machine in *Bacillus subtilis*. *Front Microbiol* 2016;**7**:1492.
668 Cavaiuolo M, Chagneau C, Laalami S *et al.* Impact of RNase E and RNase J on global
669 mRNA metabolism in the cyanobacterium *Synechocystis* PCC6803. *Front*
670 *Microbiol* 2020;**11**:1055.
671 Chambers MC, Maclean B, Burke R *et al.* A cross-platform toolkit for mass
672 spectrometry and proteomics. *Nat Biotechnol* 2012;**30**:918–20.
673 Chao Y, Li L, Girodat D *et al. In Vivo* cleavage map illuminates the central role of
674 RNase E in coding and non-coding RNA pathways. *Mol Cell* 2017;**65**:39–51.
675 Chen H, Zou W, Zhao J. Ribonuclease J is required for chloroplast and embryo
676 development in *Arabidopsis*. *J Exp Bot* 2015;**66**:2079–91.
677 Chou-Zheng L, Hatoum-Aslan A. A type III-A CRISPR-Cas system employs
678 degradosome nucleases to ensure robust immunity. *eLife* 2019;**8**, DOI:
679 10.7554/eLife.45393.
680 Commichau FM, Rothe FM, Herzberg C *et al.* Novel activities of glycolytic enzymes in
681 Bacillus subtilis: interactions with essential proteins involved in mRNA
682 processing. *Mol Cell Proteomics* 2009;**8**:1350–60.
683 Condon C, Gilet L. The metallo-β-lactamase family of ribonucleases. In: Nicholson AW
684 (ed.), *Ribonucleases*. Berlin, Heidelberg: Springer, 2011, 245–67.
685 Darty K, Denise A, Ponty Y. VARNA: Interactive drawing and editing of the RNA
686 secondary structure. *Bioinformatics* 2009;**25**:1974–5.
687 Deana A, Belasco JG. Lost in translation: the influence of ribosomes on bacterial
688 mRNA decay. *Genes Dev* 2005;**19**:2526–33.
689 Demichev V, Messner CB, Vernardis SI *et al.* DIA-NN: neural networks and
690 interference correction enable deep proteome coverage in high throughput. *Nat*
691 *Methods* 2020;**17**:41–4.

692 Durán-Figueroa NV, Piña-Escobedo A, Schroeder I *et al.* Polynucleotide
693 phosphorylase interacts with ribonuclease E through a ββαββα domain.
694 *Biochimie* 2006;**88**:725–35.
695 Ehretsmann CP, Carpousis AJ, Krisch HM. Specificity of *Escherichia coli*
696 endoribonuclease RNase E: in vivo and in vitro analysis of mutants in a
697 bacteriophage T4 mRNA processing site. *Genes Dev* 1992;**6**:149–59.
698 Even S, Pellegrini O, Zig L *et al.* Ribonucleases J1 and J2: two novel
699 endoribonucleases in *B. subtilis* with functional homology to *E. coli* RNase E.
700 *Nucleic Acids Res* 2005;**33**:2141–52.
701 Hasenöhrl D, Konrat R, Bläsi U. Identification of an RNase J ortholog in *Sulfolobus*
702 *solfataricus*: Implications for 5′-to-3′ directional decay and 5′-end protection of
703 mRNA in Crenarchaeota. *RNA* 2011;**17**:99–107.
704 Hatoum-Aslan A, Samai P, Maniv I *et al.* A ruler protein in a complex for antiviral
705 defense determines the length of small interfering CRISPR RNAs. *J Biol Chem*
706 2013;**288**:27888–97.
707 Hemm L, Miucci A, Kraus A *et al.* Interactors and effects of overexpressing
708 YlxR/RnpM, a conserved RNA binding protein in cyanobacteria. *RNA Biol*
709 2024;**21**:1–19.
710 Hofacker IL. Vienna RNA secondary structure server. *Nucleic Acids Res*
711 2003;**31**:3429–31.
712 Hoffmann UA, Heyl F, Rogh SN *et al.* Transcriptome-wide in vivo mapping of cleavage
713 sites for the compact cyanobacterial ribonuclease E reveals insights into its
714 function and substrate recognition. *Nucleic Acids Res* 2021;**49**:13075–91.
715 Hoffmann UA, Lichtenberg E, Rogh SN *et al.* The role of the 5' sensing function of
716 ribonuclease E in cyanobacteria. *RNA Biol* 2024;**21**:1–18.
717 Hotto AM, Stern DB, Schuster G. Plant ribonuclease J: An essential player in
718 maintaining chloroplast RNA quality control for gene expression. *Plants*
719 2020;**9**:334.
720 Hughes CS, Moggridge S, Müller T *et al.* Single-pot, solid-phase-enhanced sample
721 preparation for proteomics experiments. *Nat Protoc* 2019;**14**:68–85.
722 Kaltenbrunner A, Reimann V, Hoffmann UA *et al.* Regulation of pSYSA defense
723 plasmid copy number in *Synechocystis* through RNase E and a highly
724 transcribed asRNA. *Front Microbiol* 2023;**14**:1112307.
725 Kelly CL, Taylor GM, Hitchcock A *et al.* A rhamnose-inducible system for precise and
726 temporal control of gene expression in cyanobacteria. *ACS Synth Biol*
727 2018;**7**:1056–66.
728 Kelly CL, Taylor GM, Šatkutė A *et al.* Transcriptional terminators allow leak-free
729 chromosomal integration of genetic constructs in cyanobacteria.
730 *Microorganisms* 2019;**7**:263.
731 Kieper SN, Almendros C, Behler J *et al.* Cas4 facilitates PAM-compatible spacer
732 selection during CRISPR adaptation. *Cell Rep* 2018;**22**:3377–338.
733 Laalami S, Putzer H. mRNA degradation and maturation in prokaryotes: the global
734 players. *Biomol Concepts* 2011;**2**:491–506.
735 Laalami S, Zig L, Putzer H. Initiation of mRNA decay in bacteria. *Cell Mol Life Sci*
736 2014;**71**:1799–828.
737 Lehnik-Habrink M, Newman J, Rothe FM *et al.* RNase Y in *Bacillus subtilis*: a natively
738 disordered protein that is the functional equivalent of RNase E from *Escherichia*
739 *coli*. *J Bacteriol* 2011;**193**:5431–41.

740 Lehnik-Habrink M, Pförtner H, Rempeters L *et al.* The RNA degradosome in *Bacillus*
741 *subtilis*: identification of CshA as the major RNA helicase in the multiprotein
742 complex. *Mol Microbiol* 2010;**77**:958–71.
743 Levy S, Portnoy V, Admon J *et al.* Distinct activities of several RNase J proteins in
744 methanogenic archaea. *RNA Biol* 2011;**8**:1073–83.
745 Liponska A, Jamalli A, Kuras R *et al.* Tracking the elusive 5' exonuclease activity of
746 *Chlamydomonas reinhardtii* RNase J. *Plant Mol Biol* 2018;**96**:641–53.
747 Liu S-J, Lin G-M, Yuan Y-Q *et al.* A conserved protein inhibitor brings under check the
748 activity of RNase E in cyanobacteria. *Nucleic Acids Res* 2024;**52**:404–19.
749 López-Maury L, Florencio FJ, Reyes JC. Arsenic sensing and resistance system in the
750 cyanobacterium *Synechocystis* sp. strain PCC 6803. *J Bacteriol*
751 2003;**185**:5363–71.
752 Mackie GA. RNase E: at the interface of bacterial RNA processing and decay. *Nat*
753 *Rev Microbiol* 2013;**11**:45–57.
754 Marincola G, Schäfer T, Behler J *et al.* RNase Y of *Staphylococcus aureus* and its role
755 in the activation of virulence genes. *Mol Microbiol* 2012;**85**:817–32.
756 Mathy N, Bénard L, Pellegrini O *et al.* 5'-to-3' exoribonuclease activity in bacteria: role
757 of RNase J1 in rRNA maturation and 5' stability of mRNA. *Cell* 2007;**129**:681–
758 92.
759 McBride TM, Schwartz EA, Kumar A *et al.* Diverse CRISPR-Cas complexes require
760 independent translation of small and large subunits from a single gene. *Mol Cell*
761 2020;**80**:971–9.
762 Migur A, Heyl F, Fuss J *et al.* The temperature-regulated DEAD-box RNA helicase
763 CrhR interactome: Autoregulation and photosynthesis-related transcripts. *J Exp*
764 *Bot* 2021;**72**:7564–79.
765 Newman JA, Hewitt L, Rodrigues C *et al.* Dissection of the network of interactions that
766 links RNA processing with glycolysis in the *Bacillus subtilis* degradosome. *J Mol*
767 *Biol* 2012;**416**:121–36.
768 Perez-Riverol Y, Bandla C, Kundu DJ *et al.* The PRIDE database at 20 years: 2025
769 update. *Nucleic Acids Res* 2025;**53**:D543–53.
770 Pinto FL, Thapper A, Sontheim W *et al.* Analysis of current and alternative phenol
771 based RNA extraction methodologies for cyanobacteria. *BMC Mol Biol*
772 2009;**10**:79.
773 Płociński P, Macios M, Houghton J *et al.* Proteomic and transcriptomic experiments
774 reveal an essential role of RNA degradosome complexes in shaping the
775 transcriptome of *Mycobacterium tuberculosis*. *Nucleic Acids Res*
776 2019;**47**:5892–905.
777 Redko Y, Aubert S, Stachowicz A *et al.* A minimal bacterial RNase J-based
778 degradosome is associated with translating ribosomes. *Nucleic Acids Res*
779 2013;**41**:288–301.
780 Reimann V, Alkhnbashi OS, Saunders SJ *et al.* Structural constraints and enzymatic
781 promiscuity in the Cas6-dependent generation of crRNAs. *Nucleic Acids Res*
782 2017;**45**:915–25.
783 Rippka R, Deruelles J, Waterbury JB *et al.* Generic assignments, strain histories and
784 properties of pure cultures of cyanobacteria. *Microbiology* 1979;**111**:1–61.
785 Ritchie ME, Phipson B, Wu D *et al.* limma powers differential expression analyses for
786 RNA-sequencing and microarray studies. *Nucleic Acids Res* 2015;**43**:e47.
787 Scholz I, Lange SJ, Hein S *et al.* CRISPR-Cas systems in the cyanobacterium
788 *Synechocystis* sp. PCC6803 exhibit distinct processing pathways involving at
789 least two Cas6 and a Cmr2 protein. *PLoS ONE* 2013;**8**:e56470.

790 Scholz I, Lott SC, Behler J *et al.* Divergent methylation of CRISPR repeats and cas
791 genes in a subtype I-D CRISPR-Cas-system. *BMC Microbiol* 2019;**19**:147.1-
792 147.11.
793 Schwartz EA, Bravo JPK, Ahsan M *et al.* RNA targeting and cleavage by the type III-
794 Dv CRISPR effector complex. *Nat Commun* 2024;**15**:3324.
795 Scornet AL, Jousselin A, Baumas K *et al.* Critical factors for precise and efficient RNA
796 cleavage by RNase Y in *Staphylococcus aureus*. *PLoS Genet*
797 2024;**20**:e1011349.
798 Sesto N, Touchon M, Andrade JM *et al.* A PNPase dependent CRISPR System in
799 *Listeria*. *PLoS Genet* 2014;**10**:e1004065.
800 Shahbabian K, Jamalli A, Zig L *et al.* RNase Y, a novel endoribonuclease, initiates
801 riboswitch turnover in *Bacillus subtilis*. *EMBO J* 2009;**28**:3523–33.
802 Tejada-Arranz A, de Crecy-Lagard V, de Reuse H. Bacterial RNA degradosomes:
803 molecular machines under tight control. *Trends Biochem Sci* 2020;**45**:42–57.
804 Thomas PD, Ebert D, Muruganujan A *et al.* PANTHER: Making genome-scale
805 phylogenetics accessible to all. *Protein Science* 2022;**31**:8–22.
806 Tomar SK, Kumar P, Prakash B. Deciphering the catalytic machinery in a universally
807 conserved ribosome binding ATPase YchF. *Biochem Biophys Res Commun*
808 2011;**408**:459–64.
809 Trautmann D, Voß B, Wilde A *et al.* Microevolution in cyanobacteria: re-sequencing a
810 motile substrain of *Synechocystis* sp. PCC 6803. *DNA Res* 2012;**19**:435–48.
811 Vanzo NF, Li YS, Py B *et al.* Ribonuclease E organizes the protein interactions in the
812 *Escherichia coli* RNA degradosome. *Genes & Dev* 1998;**12**:2770–81.
813 Verboven S, Branden KV, Goos P. Sequential imputation for missing values. *Comput*
814 *Biol Chem* 2007;**31**:320–7.
815 Walker FC, Chou-Zheng L, Dunkle JA *et al.* Molecular determinants for CRISPR RNA
816 maturation in the Cas10-Csm complex and roles for non-Cas nucleases.
817 *Nucleic Acids Res* 2017;**45**:2112–23.
818 Yan H, Qin X, Wang L *et al.* Both enolase and the DEAD-Box RNA helicase CrhB can
819 form complexes with RNase E in *Anabaena* sp. strain PCC 7120. *Appl Environ*
820 *Microbiol* 2020;**86**:e00425-20.
821 Yegorov Y, Sendersky E, Zilberman S *et al.* A cyanobacterial component required for
822 pilus biogenesis affects the exoproteome. *mBio* 2021;**12**:10.1128/mbio.03674-
823 20.
824 Yoshihara S, Suzuki F, Fujita H *et al.* Novel putative photoreceptor and regulatory
825 genes required for the positive phototactic movement of the unicellular motile
826 cyanobacterium *Synechocystis* sp. PCC 6803. *Plant Cell Physiol*
827 2000;**41**:1299–304.
828 You MK, Shin HY, Kim YJ *et al.* Novel bifunctional nucleases, OmBBD and AtBBD1,
829 are involved in abscisic acid-mediated callose deposition in *Arabidopsis*. *Plant*
830 *Physiol* 2010;**152**:1015–29.
831 Zerulla K, Ludt K, Soppa J. The ploidy level of *Synechocystis* sp. PCC 6803 is highly
832 variable and is influenced by growth phase and by chemical and physical
833 external parameters. *Microbiology* 2016;**162**:730–9.
834 Zhang J, Hess WR, Zhang C. “Life is short, and art is long”: RNA degradation in
835 cyanobacteria and model bacteria. *mLife* 2022;**1**:21–39.
836 Zhang J-Y, Deng X-M, Li F-P *et al.* RNase E forms a complex with polynucleotide
837 phosphorylase in cyanobacteria via a cyanobacterial-specific nonapeptide in
838 the noncatalytic region. *RNA* 2014;**20**:568–79.

839 Zhang L, McSpadden B, Pakrasi HB *et al.* Copper-mediated regulation of cytochrome
840 c553 and plastocyanin in the cyanobacterium *Synechocystis* 6803. *J Biol Chem*
841 1992;**267**:19054–9.
842 Zheng X, Feng N, Li D *et al.* New molecular insights into an archaeal RNase J reveal
843 a conserved processive exoribonucleolysis mechanism of the RNase J family.
844 *Mol Microbiol* 2017;**106**:351–66.
845 Zhou C, Zhang J, Hu X *et al.* RNase II binds to RNase E and modulates its
846 endoribonucleolytic activity in the cyanobacterium *Anabaena* PCC 7120.
847 *Nucleic Acids Res* 2020;**48**:3922–34.
848 Zinchenko VV, Piven IV, Melnik VA *et al.* Vectors for the complementation analysis of
849 cyanobacterial mutants. *Russ J Gen* 1999;**35**:228–32.
850

851

852 **Figures**

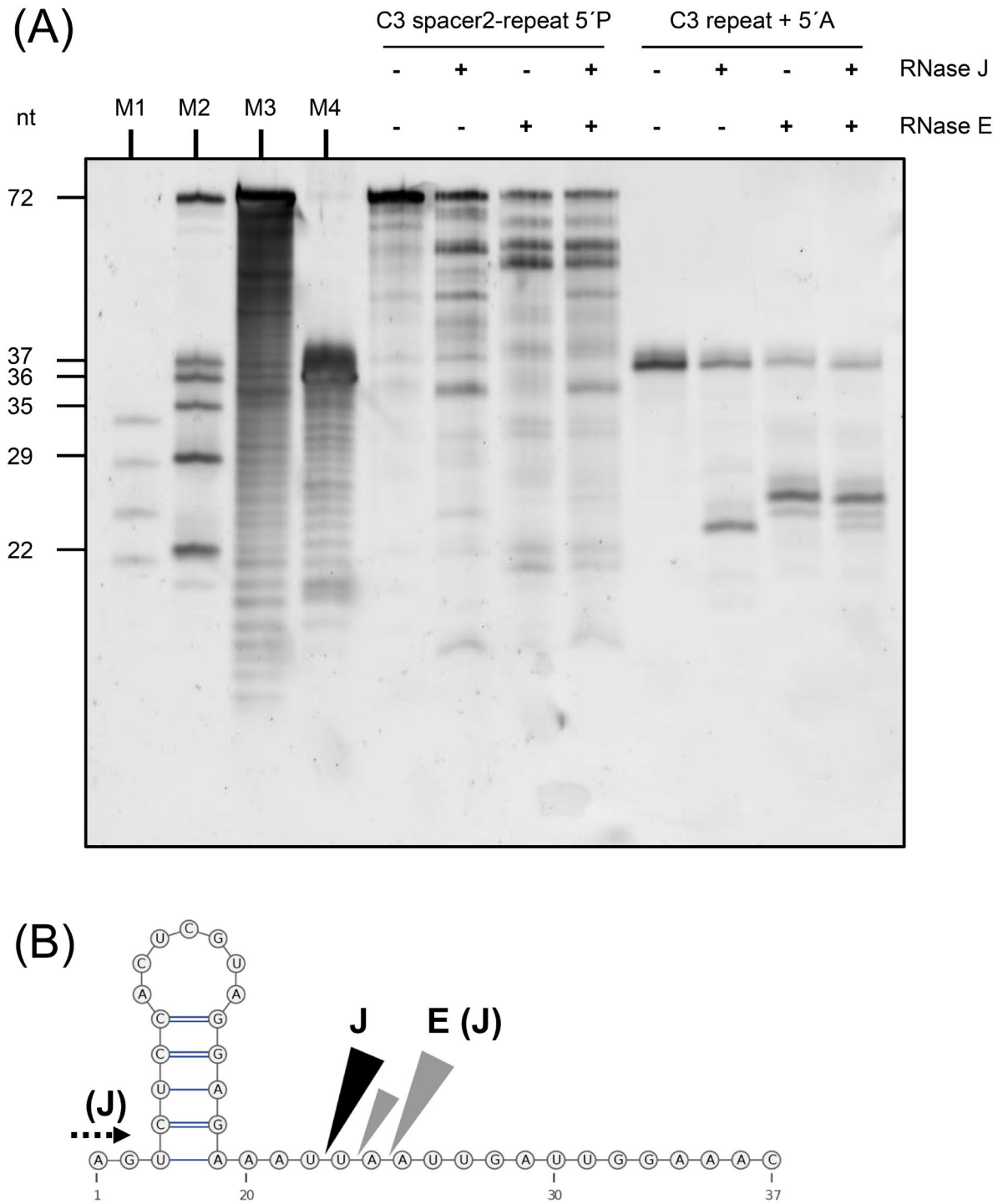

853

854 **Figure 1. *In vitro* cleavage of CRISPR3 precursor RNA by RNase J. (A)** Purified
855 recombinant RNase J and RNase E (400 ng) were incubated in various combinations
856 with 5 pmol of 5'-phosphorylated synthetic oligoribonucleotides as substrates. Lanes
857 1 to 4: Incubation with the 72 nt long CRISPR3 (C3) spacer 2-repeat RNA. Lanes 5 to

858 8: Incubation with the 37 nt long C3 repeat with an additional 5´A corresponding to the
859 final nucleotide of spacer 2. Samples were incubated for 30 min at 30°C. The reaction
860 was stopped by adding 2× RNA loading dye and denatured for 10 min at 70°C.
861 Samples were analyzed on 8 M urea-15% PAA gel. The gel was stained with SyBR
862 Gold (Invitrogen) in a 1:10,000 dilution with 0.5× Tris-Borate-EDTA buffer. Signals
863 were detected with a Laser Scanner Typhoon FLA9500 (GE Healthcare) with the
864 following settings: excitation, 473 nm; emission filter long pass blue ≥ 510 nm;
865 photomultiplier value, 400. M1: ZR small RNA ladder (17, 21, 25, and 29 nt in length,
866 Zymo research); M2: C3 ladder made of CRISPR3 repeat-related synthetic
867 oligoribonucleotides of 72, 37, 36, 35, 29 and 22 nt in length (indicated on the left);
868 M3: C3 spacer 2-repeat alkaline hydrolysis ladder; M4: C3 repeat + 5´A alkaline
869 hydrolysis ladder; nt: nucleotide; C3: CRISPR3. Note that the marker bands do not run
870 exactly according to size. **(B)** The CRISPR3 repeat RNA forms a hairpin at its 5′ end.
871 Cleavage sites by RNase J (J, black wedge) and RNase E (E, gray wedges) are
872 located within an adenylate–uridylate-rich sequence downstream of the stem-loop.
873 The twin RNase E cleavage sites match previously determined sites 13 and 14 nt from
874 the 3' end (Behler *et al.* 2018). The 2 nt shorter fragment generated by RNase J
875 compared to the RNase E main product suggests the cleavage site indicated by the
876 black wedge. However, alternatively RNase J may have cleaved the same site as
877 RNase E as an endoribonuclease, followed by 5' exonucleolytic removal of 2 nt until
878 reaching the repeat stem loop blocking further processing. This is indicated by the
879 bracketed (J) and the dashed arrow. RNA structures were predicted by RNAfold
880 (Hofacker 2003) and visualized using VARNA (Darty, Denise and Ponty 2009).

881

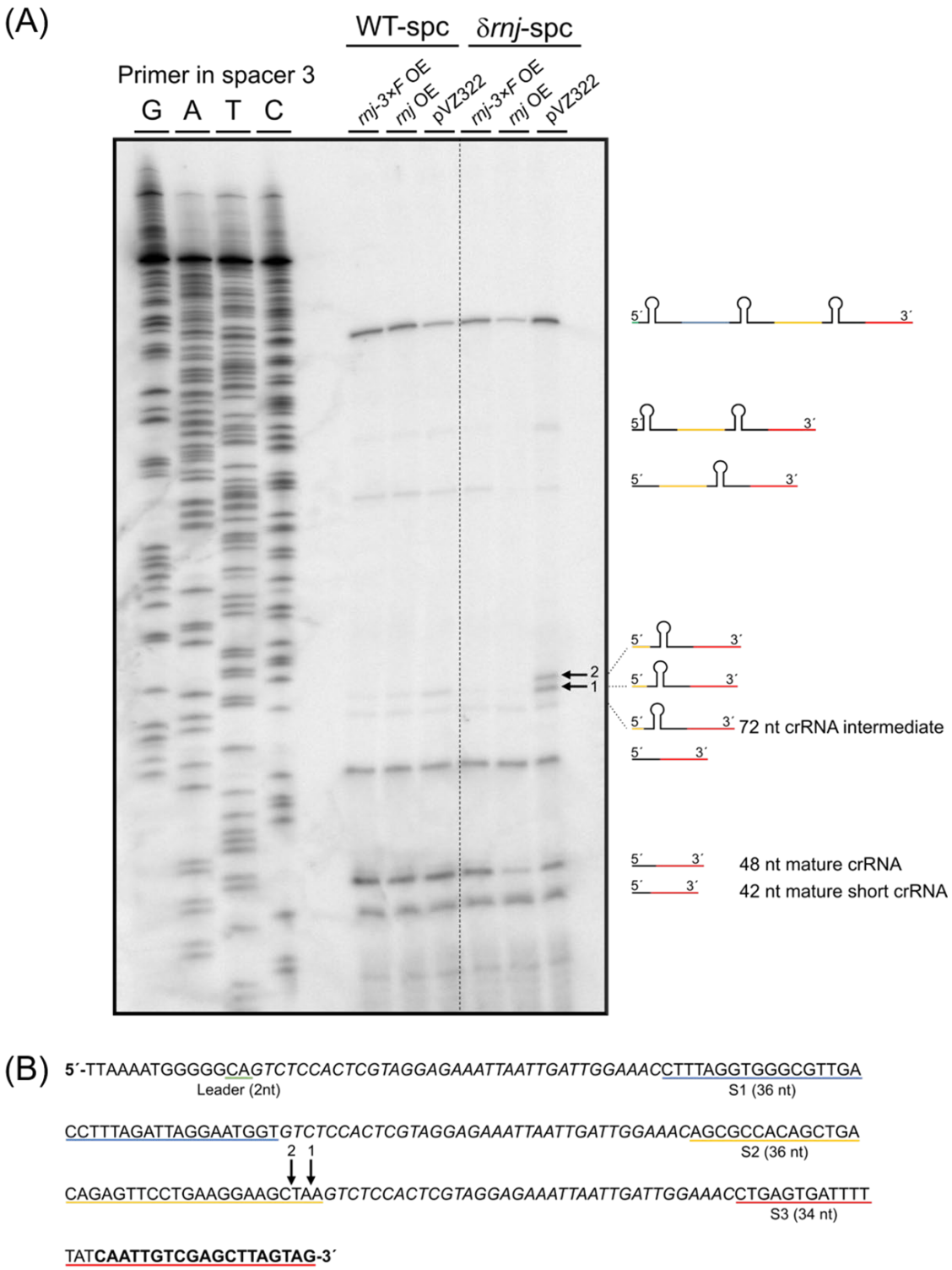

882

883 **Figure 2. Mapping of RNase J *in vivo* processing sites within CRISPR3 pre-**
884 **crRNA by primer extension**. Total RNA was isolated from the *Synechocystis rnj*
885 (*slr0551*) knock-down strain δ*rnj* carrying the empty vector pVZ322 as control,
886 pVZ322-P*petE-slr0551*, or pVZ322-P*petE-slr0551-3×flag*, as well as the

887 *Synechocystis* wild type with integrated spectinomycin cassette (WT-Spc) and
888 carrying the same set of plasmid constructs as δ*rnj*. The RNA was subjected to primer
889 extension analysis using the 5´-end-labelled oligonucleotide primer Ext_S3_rev
890 (**Table S1**) and 2 µg of total RNA per reaction. Primer extension products were
891 separated on 8.3 M urea-15% PAA gels cast in a sequencing gel device. **(A)** Mapping
892 of *in vivo* cleavage within CRISPR3 revealed the stronger accumulation of two
893 fragments in the δ*rnj* strain with decreased RNase J expression (pVZ322), labeled by
894 arrows 1 and 2. **(B)** Section of the CRISPR3 repeat-spacer array nucleotide sequence,
895 corresponding to the mapped region. The binding site of the labeled primer in spacer
896 3 necessary for reverse transcription is shown in bold. The sequence of the CRISPR3
897 repeats are in italics. The sequences of the spacers are underlined in blue for spacer
898 1 (S1), in yellow for spacer 2 (S2) and in red for spacer 3 (S3), with the length of the
899 corresponding spacer in parentheses. The sequence of the 2 nt long leader is
900 underlined in green. The cleavage sites attributed to RNase J are marked by black
901 arrows labelled 1 for the +1 and 2 for the + 3 cleavage sites close to the end of spacer
902 2.

903

904

905

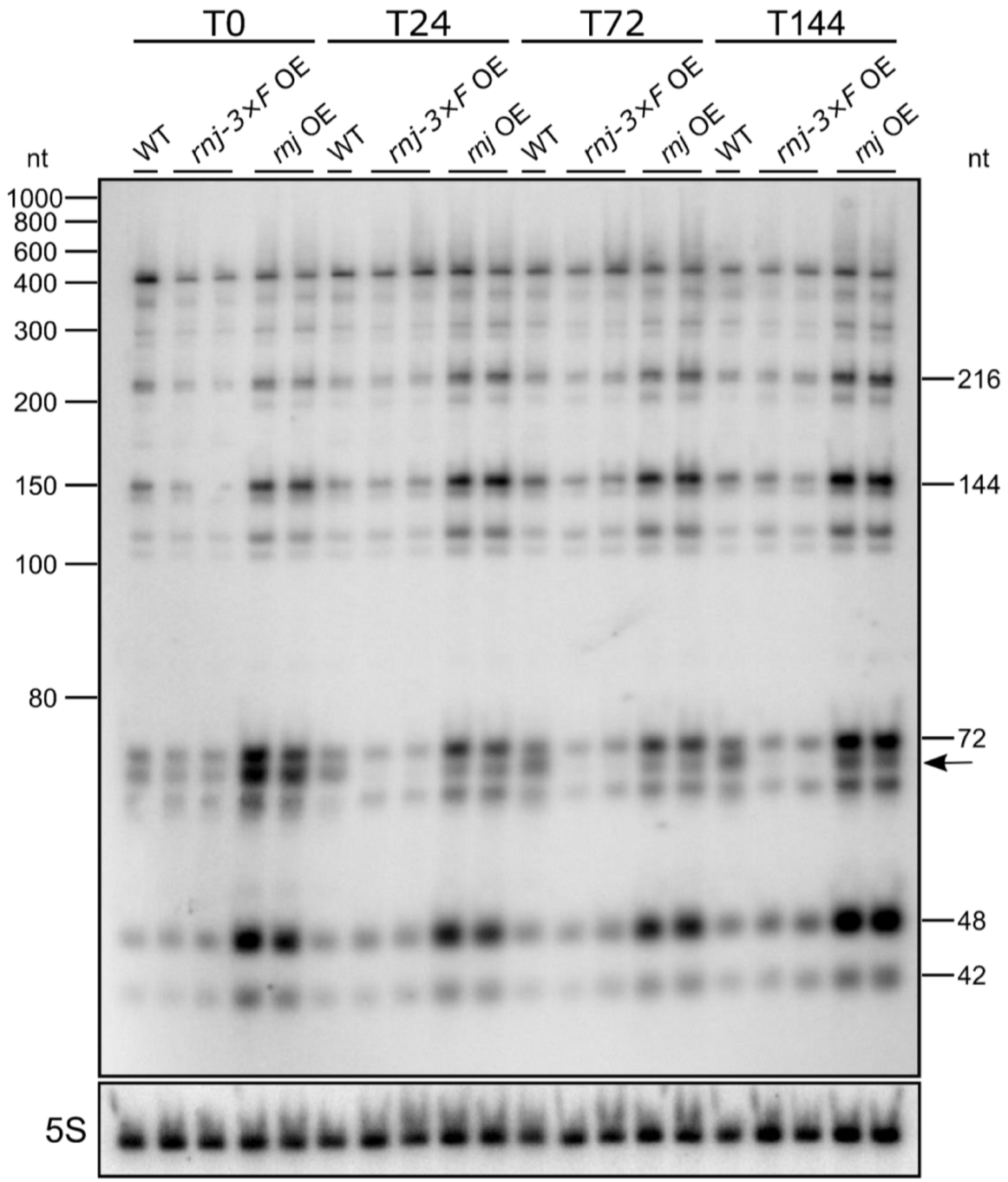

906

907 **Figure 3. CRISPR 3 crRNA accumulation in *Synechocystis* wild type and RNase**
908 **J overexpression strains**. The strains carrying pVZ322-P_{petE} constructs for the
909 expression of RNase J (*rnj* OE) or RNase J-3×FLAG (*rnj* x3F OE) and the wild type
910 strain (WT) were cultivated in copper-free BG11 medium until reaching an OD_{750} of

911 0.8. Expression of RNase J was induced with 2 μM $CuSO_4$. Samples of the cultures
912 were collected before induction (T0), and 24 h, 72 h and 144 h after induction. Ten μg
913 of total RNA isolated from each culture was separated on an 8.3M urea - 10% PAA
914 gel. For Northern hybridization, a ^{32}P-labelled transcript probe was used spanning
915 CRISPR 3 spacers 1 - 4. Hybridization of 5S rRNA is shown as the control for equal
916 loading. The black arrow marks the band at approximately 70 nt that is referred to in
917 the text. The *rnj* overexpression was verified by northern hybridization (**Supplemental**
918 **Fig. S1**).

919

920

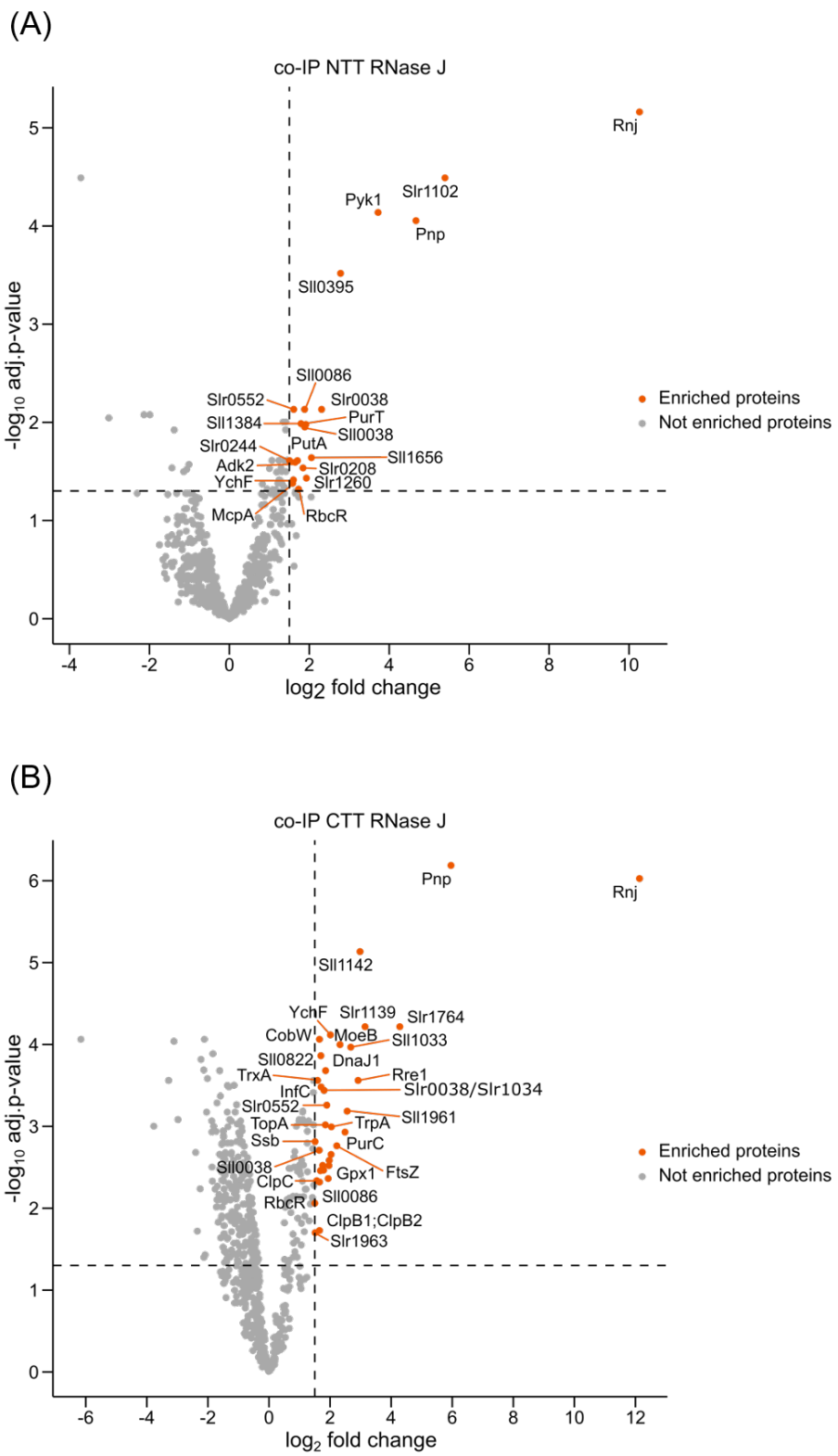

Figure 4. Co-IP experiment for the identification of interaction partners of RNase J. *Synechocystis* strains carrying pVZ322 constructs for the expression of RNase J with N- or C-terminal 3×FLAG tag, under the control of rhamnose or *petE* promoter,

925 respectively, were cultivated in the CellDEG high density system. *Synechocystis*
926 strains overexpressing GFP-3×FLAG under the control of the same promoters were
927 used as control. Protein expression was induced after 48 h of cultivation with 6 mg/ml
928 L-rhamnose or 2 µM $CuSO_4$. The equivalent of 1000 OD cells was harvested. FLAG-
929 tagged proteins were purified with M2 anti-FLAG magnetic beads and co-enriched
930 proteins were analyzed by mass spectrometry. Proteins detected in the RNase J
931 elution fraction were compared with the corresponding GFP control and visualized as
932 volcano plots based on a Limma moderated t-test with adjustment for multiple testing
933 correction. The thresholds for p value and log_2 fold change (log_2FC) were set to 0.05
934 and 1.5, respectively. Proteins with significant enrichment are indicated by orange dots
935 (enriched), while proteins which did not match the selection criteria are shown in light
936 grey (not enriched). **(A)** Co-IP with NTT RNase J. See **Supplemental Fig. S2** for the
937 Coomassie-stained SDS-PAA gel. **(B)** Co-IP with CTT RNase J. See **Supplemental**
938 **Fig. S3** for the Coomassie-stained SDS-PAA gel. Details of the proteins consistently
939 enriched in both co-IP experiments are provided in **Table 1**. The complete mass
940 spectrometry data set is provided in **Table S2**.

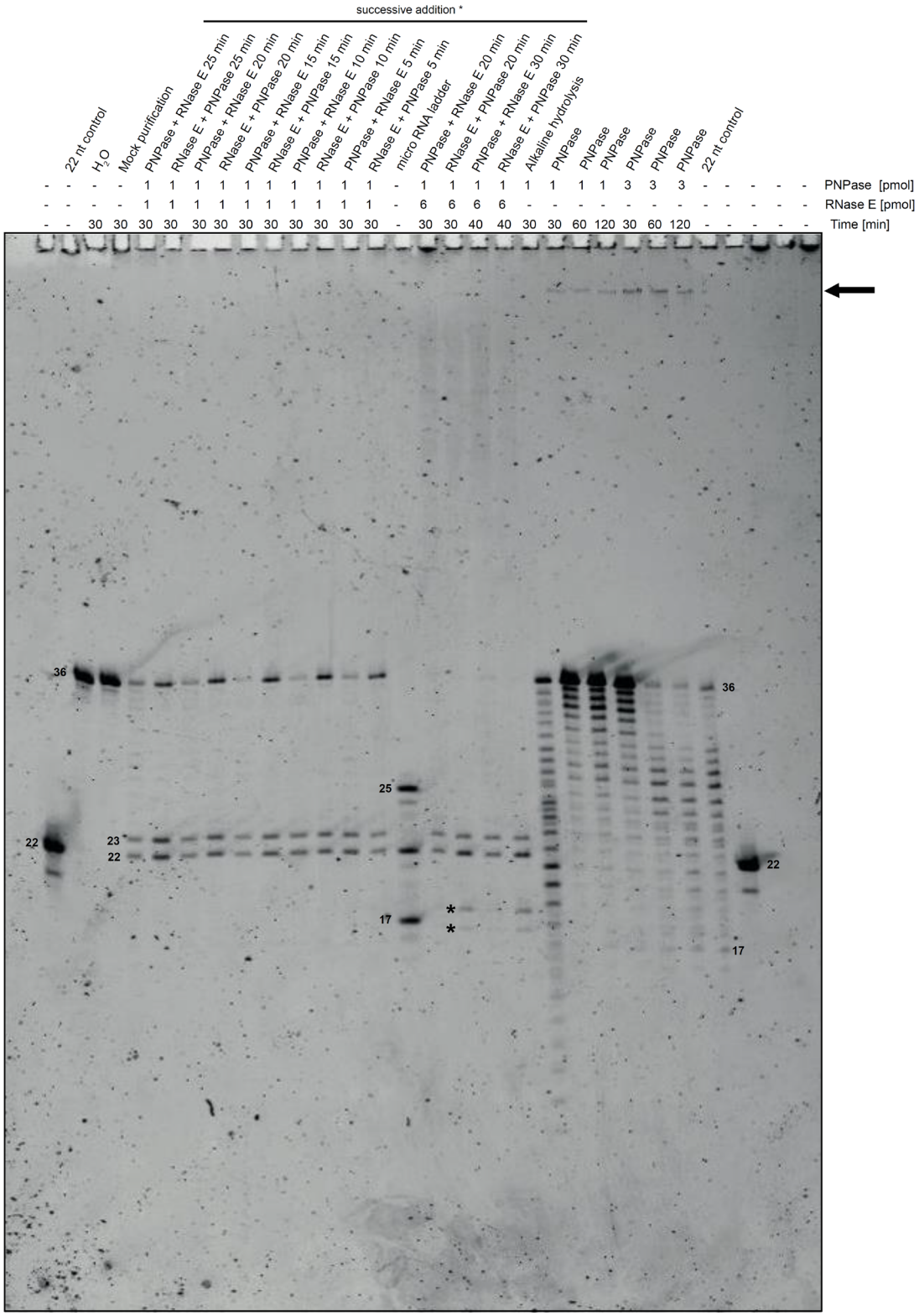

941

942 **Figure 5. *In vitro* cleavage assays with PNPase and RNase E.** Different
943 concentrations of each enzyme were used. The 5'-P CRISPR3 repeat RNA
944 oligonucleotide was used as substrate (100 ng per reaction) at 30°C with the indicated

945 enzyme amounts and incubation times. The first enzyme was added directly at the
946 beginning and the second enzyme was added after the time indicated behind. 8 M
947 urea - 15% PAA gels were used and stained with SYBR Gold. The Micro RNA ladder
948 (NEB) served as size marker. All sizes given in nt. Nuclease-free water and the mock
949 purification served as negative controls. A black arrow refers to unusual high molecular
950 products. Asterisks label unspecific products resulting from high RNase E
951 concentrations if this enzyme was added first.

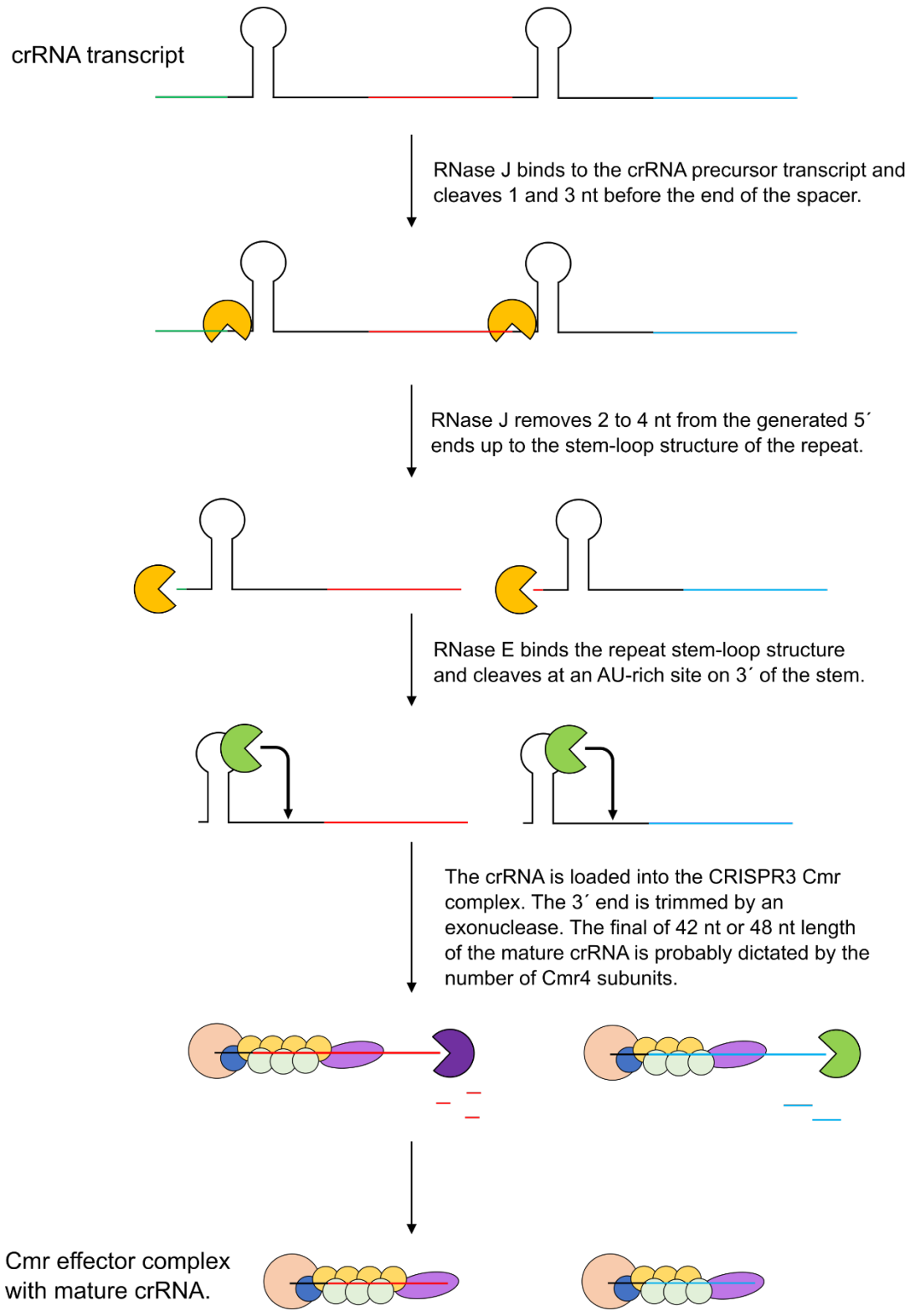

Figure 6. Model for the initiation of the maturation of CRISPR3-derived crRNAs. The transcribed CRISPR3 pre-crRNA (repeats in black) is recognized by RNase J (yellow) cleaving the transcript 1 and 3 nt from the spacer 3' end, described as the initial processing step (Scholz *et al.* 2013), followed by 5´end trimming by 2 to 4 nt until

957 reaching the stem-loop structure located at the beginning of the repeat sequence.
958 RNase E (green) then recognizes the CRISPR repeat stem-loop structure and cleaves
959 the RNA in the AU rich region downstream of the stem. This yields the mature 48 nt
960 long crRNAs with a 13 or 14 nt 5´handle (Behler *et al.* 2018). The pre-crRNA is then
961 loaded into the Cmr complex. Further 3´ trimming to the 42 nt mature crRNAs requires
962 an unknown 3´ exoribonuclease (purple). The final length of 42 nt or 48 nt (Scholz *et*
963 *al.* 2013) may be dictated by the number of Cmr4 subunits (yellow disks) attached to
964 the crRNA (Hatoum-Aslan *et al.* 2013). Both the 42 nt and 48 nt mature crRNA forms
965 accumulate *in vivo* (Scholz *et al.* 2013). The mature crRNAs are then loaded into the
966 CRISPR3-Cas protein complex.

967

968

969 ## Tables

970 **Table 1. List of proteins enriched in the co-IP with RNase J.** These are the proteins
971 enriched with both, N-terminally 3×FLAG-tagged (NTT) and C-terminally 3×FLAG-
972 tagged (CTT) RNase J and passing the selection threshold (log_2FC ≥1.5, p value
973 ≤0.05). In addition, these proteins were detected in at least three out of four replicates
974 with NTT and CTT RNase J. The columns indicate gene (G) and locus IDs, followed
975 by the log_2FC (FC) and p values (p) for the separate enrichments, uniprot accessions
976 and descriptions. Results from the MS analysis are also plotted in **Fig. 4**.

		NTT		CTT			
G	**ID**	**FC**	**p**	**FC**	**p**	**uniprot**	**Description**
rnj	*slr0551*	10.26	6.90E-06	12.13	9.41E-07	P54123	ribonuclease J (bait)
pnp	*sll1043*	4.67	8.82E-05	5.96	6.51E-07	P72659	PNPase
ebsA	*slr0038*	2.31	7.38E-03	1.80	3.63E-04	Q55457	EbsA, essential for biofilm self-suppression
pisG	*sll0038*	1.89	1.12E-02	1.64	1.96E-03	Q55448	PatA family regulator of phototaxis
sll0086	*sll0086*	1.88	7.38E-03	1.65	4.79E-03	Q55794	one-domain ArsA-like protein
rbcR	*sll0998*	1.73	4.80E-02	1.50	8.69E-03	P73123	RuBisCO transcriptional regulator
slr0552	*slr0552*	1.61	7.38E-03	1.89	5.51E-04	Q55514	gene located downstream of *rnj*
ychF	*sll0245*	1.60	3.85E-02	2.01	7.64E-05	P73886	ribosome-binding ATPase YchF
slr0244	*slr0244*	1.51	2.46E-02	2.03	2.20E-03	P72700	universal stress protein

977